Inhibition of catecholamine secretion by iron-rich and iron-deprived multiwalled carbon nanotubes in chromaffin cells

Inhibition of catecholamine secretion by multiwalled carbon nanotubes in mouse chromaffin cells: effects of iron impurity

Daniela Gavello[a,c], Ivana Fenoglio[b,c], Bice Fubini[b,c], Federico Cesano[b,c], Federica Premoselli[e], Annamaria Renna[e], Emilio Carbone[a,c,d], Valentina Carabelli[a,c,d,§]

[a] *Department of Drug Science and Technology, Laboratory of Cellular and Molecular Neuroscience, NIS Center, University of Torino, Italy*

[b] *Department of Chemistry and "G. Scansetti" Interdepartmental Center for Studies on Asbestos and other Toxic Particulates, University of Torino, Italy*

[c] *Interdepartmental Center for Nanostructured Interfaces and Surfaces, University of Torino, Italy*

[d] *National Institute of Neuroscience-Italy, Torino, Italy*

[e] *Department of Neuroscience, University of Torino, Italy*

[§] *Corresponding author:* Valentina Carabelli
Department of Drug Science and Technology
Corso Raffaello 30
10125 - Torino, Italy
tel.: +39.011.670.8488
fax: +39.011.670.8174
e-mail: valentina.carabelli@unito.it

Authors e-mail:
daniela.gavello@unito.it
ivana.fenoglio@unito.it
bice.fubini@unito.it
federico.cesano@unito.it
federica.premoselli@unito.it
annamaria.renna@unito.it
emilio.carbone@unito.it

Running title: Reduced catecholamine secretion by MWCNTs

Keywords: MWCNTs, exocytosis, chromaffin cells

Abstract

The assay of the toxic effects of carbon nanotubes (CNTs) on human health is a stringent need in view of their expected increasing exploitation in industrial and biomedical applications. Most studies so far have been focused on lung toxicity, as the respiratory tract is the main entry of airborne particulate, but there is also recent evidence on the existence of toxic effects of multiwalled carbon nanotubes (MWCNTs) on neuronal and neuroendocrine cells (Belyanskaya et al., 2009; Xu et al., 2009; Gavello et al., 2012). Commercial MWCNTs often contain large amounts of metals deriving from the catalyst used during their synthesis. Since metals, particularly iron, may contribute to the toxicity of MWCNTs, we compared here the effects of two short MWCNTs samples (< 5 μm length), differing only in their iron content (0.5 versus 0.05% w/w) on the secretory responses of neurotransmitters in mouse chromaffin cells.

We found that both iron-rich ($MWCNT_{+Fe}$) and iron-deprived ($MWCNT_{-Fe}$) samples enter chromaffin cells after 24 hours exposure, even though incorporation was attenuated in the latter case (40% versus 78% of cells). As a consequence of $MWCNT_{+Fe}$ or $MWCNT_{-Fe}$ exposure (50-263 μg/ml, 24 hours), the catecholamine secretion of chromaffin cells was drastically reduced because of the altered Ca^{2+}-dependence of exocytosis and decreased frequency of vesicle release, from 0.47 Hz (controls) to 0.11 Hz and 0.07 Hz for $MWCNT_{+Fe}$ and $MWCNT_{-Fe}$, respectively On the contrary, both MWCNTs were ineffective in changing the kinetics of neurotransmitter release of single chromaffin granules and their quantal content. Overall, our data indicate that secretion is dramatically depressed by MWCNTs, but removal of iron impurities partially attenuates this cellular “loss-of-function” in chromaffin cells and uncovers the true depressive action of nanotubes.

1. Introduction

Carbon nanotubes (CNTs) are cylindrical structures composed of carbon atoms, driving the attention of the scientific community because of their unique physico-chemical properties.

Given their potential wide use in many fields, from industry to biomedicine, it is fundamental to reveal their potential hazard. Most of the commercial CNTs contain ultrafine metal particles derived from the original growth catalyst such as Fe, Ni, Y, Co (Liu et al., 2008). Metal induced adverse effects are a real concern regarding most CNTs presently available on the market, since many studies reported that bioavailable metal impurities play a major role in CNTs-induced cytotoxicity. New purification methods could be thus a promising approach to prevent their toxicity (Liu et al., 2008). One of the main techniques used to purify CNTs surface from metal impurities is the treatment using different inorganic acids. As proposed by Nimmagadda et al. (2006), the treatment of SWCNTs with 2 M nitric acid for 10 hours significantly improves CNTs biocompatibility, reducing the amount of the catalyst residues. The main aspect to consider is that purification technologies may alter the nanotube structure (Martinez et al., 2003). Thus, the chemical composition of each nanotube preparation is of crucial importance for biological applications. Here we took advantage of a treatment with the non-oxidizing acid HCl (Liu et al., 2008), which reduces the quantity of iron impurity preserving the size and degree of nanotubes crystallinity, to assay the effects of MWCNTs on chromaffin cell secretion.

Cellular uptake and cytotoxic impact of CNTs are the main issues explored in the literature. In particular, it would be useful to develop new specific cytotoxicity assays for the rapid and reliable screening of the multitude of CNT types fabricated today (Ali-Boucetta et al., 2011). However, little is known on the effects of SWCNTs and MWCNTs on cell functions, especially on neuronal and neuronal-like preparations. In previous findings we reported that exposure of mouse chromaffin cells to MWCNTs impairs the spontaneous activity without affecting Na^+, Ca^{2+} and K^+ conductances (Gavello et al., 2012), however reports on the effects of CNTs on the functionality of the secretory apparatus are almost absent in the literature. It is proved that both single and multiwalled CNTs induce actin filaments and VE-cadherin disruption, cytotoxicity and reduced tubule formation after 24 hours exposure in

human aortic endothelial cells (Walker et al., 2009), but it is not known if this happens also in other cell types such as neurons, and how this could affect secretory vesicles trafficking. Malarkey et al. (2008) reported that water soluble SWCNTs inhibit stimulated endocytosis in rat hippocampal cultures: the long length of the nanotube seems to prevent the vesicle from closing and pinching off from the membrane, inhibiting the endocytosis.

Here we investigated the effects of well characterized MWCNTs on neuroendocrine chromaffin cells. In particular, we compared two different samples of short MWCNTs (< 5 μm length): the iron-rich ($MWCNT_{+Fe}$) and the iron-deprived sample ($MWCNT_{-Fe}$). In the latter sample the amount of iron impurities was dramatically reduced by treatment with HCl, leaving unaltered the size and crystallinity of the nanotubes. Our study is focused on the inhibitory action of MWCNTs (50-263 μg/ml) on the exocytotic properties of adrenal chromaffin cells, representing a suitable model of neuronal-like excitable cells which can massively secrete adrenaline and noradrenaline during "fight-or-flight" responses (Carabelli et al, 2003, 2007). Both MWCNT samples can translocate into the cells, as revealed by the presence of the MWCNTs both into the cytoplasm and the nucleus, thus causing a marked reduction of exocytosis without affecting Ca^{2+} channels activity, as previously reported (Gavello et al., 2012). Interestingly, even though the toxic effect on secretion is not abolished by iron removal, the iron-deprived sample ($MWCNT_{-Fe}$) affected exocytosis to a lower extent compared to the non-purified one, suggesting that iron impurities account only for part of the loss-of-function of adrenal chromaffin cells while the remaining is attributed to the toxicity of MWCNTs alone.

2. MATERIALS AND METHODS

2.1. Isolation and culture of adrenal medulla chromaffin cells

Mouse chromaffin cells (MCCs) were obtained from young C57BL/6J male mice (Harlan, Milano, Italy). All experiments were conducted in accordance with the guidelines on Animal

Care established by the Italian Minister of Health and approved by the local Animal Care Committee of Turin University.

After removal, the adrenal glands were placed in Ca^{2+} and Mg^{2+} free Locke's buffer, containing (mM): 154 NaCl, 3.6 KCl, 5.6 NaHCO3, 5.6 glucose, and 10 HEPES (pH 7.3, at room temperature). Glands were then decapsulated to separate the medullas from the cortex. Enzymatic digestion was achieved by keeping the medulla for 20 min at 37°C into a DMEM solution enriched with 0.16 mM Lcysteine, 1 mM $CaCl_2$, 0.5 mM EDTA, 20 U/ml of papain (Worthington Biochemical, Lakewood, NJ, USA), 0.1 mg/ml of DNAse (Sigma, Milan, Italy). The digested glands were then washed with a solution containing DMEM, 1 mM $CaCl_2$,10 mg/ml BSA and resuspended in 2 ml DMEM supplemented with 15% fetal bovine serum (FBS) (Invitrogen, Grand Island, NY, USA). Isolated chromaffin cells were obtained after mechanical disaggregation of the glands. Cells were then incubated at 37°C in a water-saturated atmosphere with 5% CO_2 and used within 2-4 days after plating.

Rat chromaffin cells were prepared according to the same protocol (Carabelli et al., 2007) and used limitedly to the electron microscopy trials.

2.2. Preparation of MWCNTs

Pristine multi walled carbon nanotubes ($MWCNT_{+Fe}$) were purchased by Mitsui Chemicals (Kawasaki-Shi, Japan); this sample was then shortened by grinding in an oscillatory agate ball mill for 6 hours. One aliquot of was suspended in 1 M HCl to dissolve iron impurities and the suspension stirred at room temperature for 10 days. These obtained purified MWCNTs ($MWCNT_{-Fe}$) were then recovered by centrifugation, washed with distilled water and dried (Liu et al., 2008).

2.3. Surface area

The surface area of MWCNTs was measured by means of the BET method based on N_2 adsorption at -196°C (Micrometrics ASAP 2010).

2.4. Morphology

The dimension of MWCNTs has been evaluated by means of atomic force microscopy (AFM) and transmission electron microscopy (TEM). The morphology and the statistical evaluation of diameters and lengths of the MWCNT fragments were obtained by considering a population of 300 data each, coming from AFM scans (10x10, 5x5 and/or 2x2μm in size) and from low resolution TEM images (4000X and 25000X as magnification, respectively) of the ground sample before and after the removal of iron. AFM images were collected in non-contact mode by a Park Systems XE-100 on MWCNTs dispersed on mica from a diluted and sonicated MWCNT/IPA solution, while TEM images were collected by a JEOL 3010-UHR TEM instrument operating at 300 kV.

2.5. Elemental analysis

Metallic contamination was quantified after calcination of the different MWCNT preparations and re-suspension of the residue in concentrated HCl. The concentration of iron in the solution was quantified. The analysis of the obtained solution was performed by atomic emission-inductively coupled plasma (AE-ICP) spectrometry (IRIS II Advantage/1000, Thermo Jarrel Ash, Franklin. MA).

2.6. Evaluation of potentially bioavailable iron

This test was performed to evaluate the amount of iron ions exposed at the surface of the MWCNTs, according to previously described procedures (Liu et al., 2008; Lund and Aust, 1990; Martra et al., 2003). To this purpose, a strong Fe^{2+} ions chelator (ferrozine) and a reducing agent (ascorbic acid) were used to extract iron ions. 25 mg of the powders were

incubated in 10 ml of a 3 mM solution of ascorbic acid and ferrozine. After 10 days an aliquot of the supernatant was withdrawn after centrifugation and the concentration of iron evaluated by measuring the absorbance at 562 nm (typical of the complex ferrozine-Fe(II)) by means of an UV/Vis spectrophotometer (Uvikon, Kontron, Eching, Germany).

2.7. Raman Spectroscopy

Micro-Raman spectra were acquired using an integrated micro/macro Raman system which includes a Horiba Jobin Yvon HR800 microspectrometer, an Olympus BX41 microscope and a CCD air-cooled detector. A polarized solid state Nd 80 mW laser operating at 532.11 nm was used as the excitation source. Calibration of the instruments was performed by measuring the Stokes and anti-Stokes bands and checking the position of the Si band at ± 520.7 cm^{-1}. Each spectrum was acquired using a 100X objective, resulting in a laser beam size at the sample in the order of 2 mm. To optimize the signal to noise ratio, spectra were acquired using 10 scans of 10 seconds for each spectral region. In order to produce strong signals without inducing surface alteration due to the heat, a filter with optical density d = 0.6 was used. The software LabSpec 5 (Horiba Jobin Yvon) was used to analyze the spectra. The I_D/I_G value is the ratio of the intensities of two bands designated as D (1340 cm^{-1}) and G (1570 cm^{-1}) which correspond respectively to structural defects and to the tangential in-plane stretching vibration of the carbon-carbon bonds within the graphene sheets.

2.8. Dispersion of MWCNTs in the culture media

The MWCNTs were suspended in the culture media described below at the concentration of 263 mg/l. The suspensions were sonicated twice for 2 minutes in ice (100 W, 20 kHz, Sonoplus, Bandelin, Berlin, Germany).

Average hydrodynamic size of MWCNTs in the culture media has been evaluated by means of dynamic light scattering (DLS) (Zetasizer Nano–ZS, Malvern Instruments, Worcestershire,

UK). The measurement was repeated after 15 minutes to evaluate the stability of the suspension. Since in the DLS technique particles larger than 1 μm are not detected, optical microscopy was also used to detect the presence of large aggregates.

2.9. Electron microscopy

Rat chromaffin cells were cultured on Aclar Fluoropolymer film (Electron Microscopy Sciences, USA) and were subjected to the protocol already described (Gavello et al., 2012). Briefly, 24 h after treatment, cells were fixed with 2% glutaraldehyde, post-fixed in 1% osmium tetroxide and then embedded in Epon-Araldite. Ultrathin sections (80–100 nm) were cut with a diamond knife on an ultramicrotome (Leica Microsystems, Germany), collected on Pioloform-coated single slot grids (Electron Microscopy Sciences, USA) and stained with uranyl acetate and lead citrate. Sections were examined in a JEM-1010 electron microscope (Jeol, Japan) equipped with a side-mounted CCD camera (Mega View III; Soft Imaging System, Germany). Approximately, 60 chromaffin cells treated with $MWCNTs_{-Fe}$ for 24 h were randomly examined to determine the presence of nanotubes inside the cytoplasm. Approximately, 60 rat chromaffin cells treated with $MWCNTs_{-Fe}$ (263 μg/ml) for 24 h were randomly examined to determine the presence of nanotubes inside the cytoplasm. These results were then compared with our previous data on chromaffin cells treated with $MWCNTs_{+Fe}$ (Gavello et al., 2012). We also evaluated the percentages of single nanotubes or agglomerates of nanotubes internalized into the cells.

2.10. Electrophysiological recordings

Electrophysiological experiments were performed in the whole-cell perforated configuration by using an EPC-10 amplifier and Patch Master software (HEKA-Elektronic, Germany) as described previously (Marcantoni et al., 2009). Patch-clamp pipettes were made using borosilicate glass (Kimax 51; Witz Scientific, OH, USA) and filled with an internal solution

containing (mM): 135 $CsMeSO_3$, 8 NaCl, 2 $MgCl_2$, 20 HEPES and amphotericin B (500 μg/ml) (pH 7.3 using CsOH). Pipettes' series resistance was 1-2 MΩ. The external bath contained (mM): 4 TEACl, 126 NaCl, 10 $CaCl_2$, 4 KCl, 2 $MgCl_2$, 10 Glucose, 10 HEPES (pH 7.4 with NaOH). All the experiments were performed at room temperature. Ca^{2+} currents were sampled at 10 kHz and filtered at 2 kHz.

Depolarization-evoked exocytosis was measured as membrane capacitance increases (ΔC_m) after depolarizing pulses (Carabelli et al., 2003). Ca^{2+} currents were evoked by applying step depolarizations (100 ms duration), from an holding potential of –80 mV, to fixed potentials. Superimposed on the square pulse, a sinusoidal wave function (1000 Hz, 25 mV amplitude) was applied in order to monitor membrane capacitance increases following the depolarizing steps using the Lockin extension of the Patchmaster software. Fast capacitive transients due to depolarizing pulses were minimized online by the patch-clamp analog compensation. Series resistance was compensated by 80% and monitored during the experiment. The amount of Ca^{2+} entering the cells during a depolarization (quantity of charge in pC) was calculated as the time integral of the Ca^{2+} current.

2.11. Amperometric recordings

Amperometric recordings were performed by means of commercial carbon fibres (ALA Scientific Instrument Inc., Westbury, NY, USA) as previously described (Carabelli et al., 2010, 2007). Before each trial, carbon fibers were cut at an angle of 45°, inserted into the head-stage of a EPC-10 HEKA amplifier, polarized to +800 mV and finally positioned next to the cell membrane. Mouse chromaffin cells were kept in saline solution, containing (mM): 130 NaCl, 2 $MgCl_2$, 10 glucose, 10 HEPES, 10 $CaCl_2$, 4 KCl. Then exocytosis was stimulated by using a KCl-enriched solution, containing (mM): 100 NaCl, 2 $MgCl_2$, 10 glucose, 10 HEPES, 10 $CaCl_2$, 30 KCl. Amperometric currents were sampled at 4 kHz, low-pass filtered at 1 kHz, monitored over 120 s. This same stimulation protocol has been followed either for control

cells, and after incubation with MWCTNs. Recordings have been analyzed by using IGOR macros (Wave-Metrics, Lake Oswego, OR, USA) (Carabelli et al., 2007).

3. RESULTS

3.1. Preparation and characterization of MWCNTs

Short $MWCNT_{+Fe}$ were obtained by grinding a sample of commercial MWCNTs. Ground MWCNTs ($MWCNT_{+Fe}$) are AFM imaged in Figure 1a. They exhibited a mean length of 1.12 μm and iron as main impurity (0.5%) in large part accessible to the solvent (84%) and therefore potentially active toward cells (Table 1). Several protocols have been proposed to remove metal contaminants from MWCNTs (Cho et al., 2009) that include chemical treatments with oxidising acids (HNO_3, H_2SO_4) or thermal treatments at high temperature in inert atmosphere (Bougrine et al., 2001; Fenoglio et al., 2008). These treatments also affect the structure of CNTs either increasing or decreasing the amount of defects. Since defects have been reported to modulate the toxicity of CNTs (Fenoglio et al., 2008; Muller et al., 2008), the role of iron impurities in the toxicity of CNTs would be unambiguously determined only by comparing samples having a similar amount of defects. Thus, we opted for a protocol which did not modify the structure of CNTs. Following Cho et al. (2009) we used the non-oxidizing acid HCl that at room temperature completely removed the potentially available iron impurities, leaving almost unaltered the dimensions of nanotubes. There was, in fact, only a very small increase of diameter and length after the treatment, which results in a slightly higher surface area of $MWCNT_{+Fe}$ (Table 1). In Fig. 1 representative images of MWCNTs are shown. Both control (panel ***a***) and HCl-treated MWCNTs (panel ***b***) exhibit diameter and length similarly distributed around their mean value (panel ***c*** and ***d***).

The treatment used to remove iron also left unaltered the microscopic structure of the nanotubes, as proved by the Raman spectra (Fig. 2). The Raman spectra of $MWCNT_{+Fe}$ were characterized by three main bands (Fig. 2, black dotted line). The two bands at 1575 and 2686

cm^{-1} (G and G') are due to the tangential stretching of graphitic sp^2 materials. The band at 1346 cm^{-1} (D), together with a small shoulder at 1614 cm^{-1} (D') originate from the structural disorder of amorphous carbon or defective graphene sheets (Bertarione et al., 2009, Cesano et al., 2008). The intensity ratio between the disorder-induced D-band and the Raman allowed G band (I_D/I_G) is generally used to quantify the disorder in graphenic materials (Cravotto et al., 2011; Dresselhaus et al., 2010). The low I_D/I_G ratio found for $MWCNT_{+Fe}$ (Table 1) is indicative of a highly crystalline structure, thus confirming what observed in TEM analysis. The Raman spectra of $MWCNT_{-Fe}$ fully overlapped the one of the untreated sample (Fig. 2, gray line) and the I_D/I_G ratio was similar suggesting that the HCl treatment does not affect the graphitic structure of CNTs.

3.2. Dispersion on MWCNTs in cell media

Being highly hydrophobic, MWCNTs are weakly dispersed in aqueous media. However, in the presence of proteins acting as surfactant, stable suspensions can be obtained (Elgrabli et al., 2007). MWCNTs were dispersed directly in the cellular media following sonication. The degree of dispersion and the stability of the suspensions were measured by using two complementary techniques, DLS and optical microscopy (Table 1, Fig. 3). A single peak, corresponding to agglomerates having a mean equivalent hydrodynamic diameter of 300-400 nm was obtained for both samples. As expected, the dispersions were characterized by a high degree of poly-dispersity (Table 1). In Fig. 3A are reported the DLS curves of the suspension of $MWCNT_{-Fe}$ in cell media recorded for a period of 15 minutes, which is a sufficient period for a correct dosage. No changes were detectable both in the form and position of the peak. Since DLS detection has an upper limit of 1 μm of diameter, the presence of larger aggregates was evaluated by optical microscopy. $MWCNTs_{-Fe}$ appeared uniformly distributed in the suspension with some aggregates having mean diameters of 0.3-10 μm. Similar results were obtained for $MWCNT_{+Fe}$, as previously shown (Gavello et al., 2012).

3.3. MWCNTs$_{-Fe}$ are less internalized than MWCNTs$_{+Fe}$

A set of electron microscopy trials has been performed to investigate whether MWCNTs$_{-Fe}$ could be internalized into rat chromaffin cells (RCCs), as previously demonstrated for MWCNTs$_{+Fe}$ (Gavello et al, 2012). To this purpose, ultrathin sections of RCCs, exposed for 24 hours to MWCNTs$_{-Fe}$ (263 μg/ml), were analyzed. Representative images of chromaffin cells under control conditions and after exposure to MWCNTs$_{-Fe}$ and MWCNTs$_{+Fe}$ are shown in Fig. 4a, 4b and 4d, respectively. MWCNTs$_{-Fe}$ were able to cross the membrane and enter the cytoplasm of the cells as well as into the nucleus (Fig. 4c). Nanoparticles were included in 40% of cases (Fig. 4e), with a predominance of single nanotubes rather than aggregates (70% and 30%, respectively). Thus, by comparing the percentage of internalization between iron-rich and iron-deprived MWCNTs, we found that it occurs with a lower extent for MWCNTs$_{-Fe}$ (40% versus 78%). MWCNTs can be internalized inside the cells as single nanotubes or as aggregates. Fig. 4f shows that chromaffin cells treated with iron-deprived MWCNTs presented, in most cases, single internalized nanotubes (70%), while the occurrence of single nanotubes and aggregates was limited to 30%.

3.4. MWCNTs reduce secretory responses without affecting Ca^{2+} entry

MWCNT$_{+Fe}$ have been shown to severely impair the spontaneous firing activity of mouse chromaffin cells (MCCs) in a dose-dependent way, lowering both the cell membrane input resistance and the number of spontaneously active cells. Spontaneously active cells after MWCNTs exposure had more depolarized resting potentials, higher firing frequency and unaltered voltage-gated Ca^{2+}, Na^{+} and K^{+} current amplitudes (Gavello et al., 2012). Since chromaffin cells are in vivo activated by splancnic nerve stimulation to massively release catecholamines into the bloodstream (Marcantoni et al., 2010; Vandael et al., 2010; 2012), here we studied whether MWCNTs exposure could affect secretory responses as well, and whether

this loss of function was also dependent on the presence of iron impurities. To this purpose, MCCs were exposed for 24 hours to either iron-rich ($MWCNTs_{+Fe}$) or iron-deprived ($MWCNTs_{-Fe}$) nanotubes (Gavello et al., 2012). Secretory responses were investigated both at a macroscopic level, by measuring the total secretion from the whole cell, and by studying the kinetics and amplitude of single quantal exocytic events associated to the release of chromaffin granules content. In order to increase the sample homogeneity, when measuring the effects of MWCNTs on secretion, we selectively patch-clamped those cells which appeared covered by MWCNTs. Although this could not be taken as an index of nanoparticles internalization, it ensured at least the presence of nanoparticles close to the cell membrane. Fig. 5a (top) shows representative images of chromaffin cells under control conditions and after exposure to MWCNTs. The cells surrounded by nanotubes were selected for the electrophysiological trials (arrows).

Following this, in a first series of experiments, secretory responses were measured as membrane capacitance increases (ΔC) after 100 ms depolarization to +10 mV, with the aim of investigating the Ca^{2+}-dependent secretion of the whole cell (Fig. 5a, bottom). Experiments under control conditions and after exposure to MWCNTs have been both performed using chromaffin cells of the same age.

Relevant inhibitory effects were detected on Ca^{2+}-dependent secretory responses by both iron-rich and iron-deprived MWCNTs with respect to controls, (Fig. 5a, b). On average, under control conditions, the Ca^{2+} entry during the 100 ms depolarizing pulses to +10 mV caused secretory responses of 55.6 ± 7.4 fF (n = 25 cells) (Marcantoni et al., 2009), while after CNTs exposure, secretion decreased to 36.8 ± 1.7 fF with $MWCNTs_{-Fe}$ (n = 54 cells) and to 25.5 ± 1.3 fF with the $MWCNTs_{+Fe}$, (50 μg/ml) (n = 42 cells) ($p< 0.05$, one way ANOVA followed by Bonferroni post hoc analysis). Thus, removal of iron impurities from MWCNTs significantly attenuate the MWCNTs-induced inhibition of chromaffin cell secretion (Fig. 5b), by assuming comparable distributions of nanotubes. Interestingly, higher MWCNTs concentrations (263

μg/ml) had no further inhibitory effects on secretion: mean ΔC remained at 35.1 and 29.8 fF, respectively for iron-deprived and iron-rich samples ($p > 0.1$, Fig. 5b).

The decrease of the capacitance responses by MWCNTs was further investigated by comparing the ΔC distribution among controls and cells exposed to $MWCNTs_{+Fe}$ and $MWCNTs_{-Fe}$ (50 μg/ml). Under control conditions the capacitance increase followed a bimodal distribution, that was best fitted by two-gaussian distributions, indicating that secretory responses, on average, contribute by increasing the membrane surface by 26 up to 75 fF (mean values of the two Gaussian distributions). After cell incubation with $MWCNTs_{-Fe}$, the two peaks of capacitance were both shifted towards lower values (17 and 34 fF), while in the presence of $MWCNTs_{+Fe}$ the distribution was unimodal with a peak at 16 fF. Thus, $MWCNTs_{-Fe}$ act by mainly reducing the population of large ΔC secretory responses, which are nearly abolished in the presence of $MWCNTs_{+Fe}$ (Fig. 6a and b).

The progressive shift of the peak distribution toward small capacitance changes and the complete loss of large secretory responses with $MWCNTs_{+Fe}$ was unexpected but clearly proved that the effects of $MWCNTs_{-Fe}$ derived from pooling cells with internalized nanoparticles and not from cell mixtures with and without internalized $MWCNTs_{-Fe}$. In the latter case, pooling cells with no internalized nanotubes (control-like) would have produced higher capacitance values and a more prominent bimodal distribution in the presence of $MWCNTs_{-Fe}$ that we did not observe. In conclusion, the results of Fig. 6 suggest that iron impurities are mainly responsible for most of the large ΔC decrease and consequent key alteration of chromaffin cell functionality, while the MWCNTs *per se* account for the minor decrease of the small capacity changes (from 26 to 17 pF).

In order to exclude that the reduced secretion could be associated to a limited Ca^{2+} influx, we compared the quantity of charge (Ca^{2+} ions) entering through voltage-gated Ca^{2+} channels during +10 mV depolarizing pulses, and found that this parameter was not affected by MWCNTs exposure (50 μg/ml for both samples). For untreated cells, the mean quantity of

charge was 21.6 ± 1.4 pC and remained unaltered ($p > 0.1$, one way ANOVA followed by Bonferroni post hoc analysis) after 24 hours incubation with $MWCNTs_{-Fe}$ (19.6 ± 0.8 pC) or $MWCNTs_{+Fe}$ (19.9 ± 0.8 pC). These results are in good agreement with our previous data (Gavello et al., 2012) and suggest that Ca^{2+} charge entering through voltage-gated Ca^{2+} channels is not affected by MWCNTs, independently of iron impurities. Ca^{2+} entry was preserved also when increasing the MWCNTs concentration up to 263 μg/ml (Fig. 5c).

Overall, our data demonstrate two critical issues on the toxic effects of CNTs: 1) chromaffin cells secretion is severely impaired by exposure to CNTs despite Ca^{2+} charge remained unaltered, and 2) the presence of iron impurities can largely attenuate the secretory response.

3.5. Altered Ca^{2+}-dependence of exocytosis caused by MWCNTs exposure

Next, we investigated the Ca^{2+}-dependence of exocytosis, to assess whether the same quantity of charge (Ca^{2+} ions) could differently trigger secretion under control conditions and after exposure to MWCNTs. To this purpose, capacitance increases caused by depolarizing pulses were plotted versus the corresponding quantity of charge. In control conditions, linear regression gave 1.8 ± 0.3 fF/pC, which decreased to 1.3 ± 0.1fF/pC with 50 μg/ml $MWCNTs_{-Fe}$ and to 1.0 ± 0.1 fF/pC with 50 μg/ml $MWCNT_{+Fe}$. Linear regression under control conditions differs from $MWCNTs_{-Fe}$ by 1 standard deviation and from $MWCNTs_{+Fe}$ by 2 standard deviations, indicating that both nanotubes alter the Ca^{2+} coupling to the secretory apparatus, the effect being more pronounced in the presence of iron-rich MWCNTs (Fig. 6c).

3.6. MWCNTs reduce the frequency of quantal secretory events without affecting their time course and amplitude

Our findings suggest that reduced secretion is mainly ascribed to an altered coupling of Ca^{2+} to the functionality of the secretory apparatus. Furthermore, to assess whether MWCNT could also alter the kinetics and amplitude of single quantal events, we measured the corresponding

amperometric spikes following exposure to $MWCNTs_{-Fe}$ and $MWCNTs_{-Fe}$ (50 μg/ml). Amperometric currents associated to the oxidation of released catecholamines from chromaffin granules were evoked by a KCl-enriched external solution (see paragraph 2.11) and measured for 120 s. As shown in Table 2, parameters characterizing single quantal events (see Carabelli et al. 2007) were not significantly modified, with the unique exception of spike frequency, which was significantly reduced by either by $MWCNTs_{-Fe}$ or $MWCNTs_{+Fe}$ (Fig. 7). It is worth noticing that dimensions of the chromaffin granules as well as their catecholamine content were preserved, as indicated by the mean $Q^{1/3}$ (Marcantoni et al., 2009) which was unaltered under the three experimental conditions: 0.56 $pC^{1/3}$ (controls), 0.54 ($MWCNTs_{-Fe}$) $pC^{1/3}$ and 0.53 $pC^{1/3}$ ($MWCNTs_{+Fe}$). Also the kinetic parameters of the spikes (I_{max}, $t_{1/2}$, m, t_p) were not affected by MWCNTs (see Table 2 for details), indicating that the time course of quantal catecholamine release was not affected by the nanotubes. To this purpose, representative spikes under the three conditions are shown at higher time resolution in Fig. 7. However, it is important to notice that the frequency of quantal events was severely impaired, from 0.47 to 0.11 Hz for $MWCNT_{-Fe}$ ($p< 0.001$) and to 0.07 Hz for $MWCNTs_{+Fe}$ ($p< 0.001$, one way ANOVA followed by Bonferroni post-hoc comparison). Overall these data demonstrate that an impaired number of secretory events occurs after MWCNTs exposure (Pacurari et al., 2011). The reduced frequency of secretory events together with the altered coupling of Ca^{2+} ions to the secretory apparatus functionality, can fully account for the impaired catecholamine release from chromaffin cells following MWCNTs treatment.

4. DISCUSSION

We have shown that when tested for their toxicity on *in vitro* neuronal-like cell functionality, two samples of MWCNTs, with high and low iron impurities but equal diameter, length and amount of defects, exhibit different degree of cell internalization and produce significantly different inhibitory effects on neurosecretion. The MWCNTs containing bioavailable iron

impurities have higher probability of being internalized within chromaffin cells and drastically decrease the quantity of released catecholamines mainly by reducing the frequency of single secretory events but preserving their size and time course. The MWCNTs purified from bioavailable iron produce similar reductions on catecholamine secretion, but at lower extent. On this issue we have clearly shown that the extent of the reduction is not due to a lower percentage of nanotubes internalization (40 % versus 78 %) but rather to the reduced amount of iron potentially released (Fig. 6), or to their aggregated form when internalized (see below). Moreover, we provided evidence that both samples of MWCNTs reduce the Ca^{2+}-dependent catecholamine secretion without affecting Ca^{2+} fluxes.

Since removal of bioavailable metals could be a promising strategy to reduce CNTs toxicity and related health risk (Kagan et al., 2006, Liu et al., 2008; Nimmagadda et al., 2006; Pulskamp et al., 2007), we performed a purification of MWCNTs to remove the iron impurities that are constitutively present in the nanomaterial. Several protocols may be used to remove metallic contaminants from CNTs, such as the treatments with mixture of oxidant acids or the thermal treatments. However, these procedures also affect the structure of CNTs by inserting oxygenated functionalities at the surface or by annealing structural defects (Wang et al., 2011). We were interested in modifying only the iron content and therefore applied a soft treatment with a non-oxidizing strong acid (HCl). This procedure efficiently removed the bioavailable iron (Table 1), leaving unaltered the crystalline degree and the morphology of the MWCNTs. Metal impurities may be exposed at the surface of CNTs or embedded inside the tubes. Under a toxicological point of view, only the metals exposed to the solvent (potentially bioavailable) are expected to affect cell responses (Liu et al., 2008). Therefore, a sample of MWCNTs containing iron and a sample HCl-treated (with minimal metal traces) were tested for the amount of potentially removable (bioavailable) iron (Liu et al., 2008). After the HCl treatment, the amount of iron potentially bioavailable was negligible (Table 1).

In order to examine the toxic effects of the two samples we first tested their capability of translocation through the biological membranes using electron microscopy trials. Cellular uptake of $MWCNTs_{-Fe}$ by rat chromaffin cells occurred in 40% of cases, while increased to 78% for $MWCNTs_{+Fe}$ (Gavello et al., 2012); furthermore $MWCNTs_{-Fe}$ do not disrupt the internal organization and are present mostly as single elements rather than as nanotubes aggregates. We then examined the toxic effect of MWCNT on chromaffin cell functionality, by measuring the Ca^{2+}-dependent exocytosis. Reduced catecholamine secretion is associated to a lower frequency of granules release together with an altered Ca^{2+}-dependence of exocytosis after MWCNTs treatment, both effects being more pronounced for the iron-rich sample ($MWCNTs_{+Fe}$). These findings are in good agreement with those reported by Cheng et al. (2009), showing that MWCNTs toxicity is due to the nanotubes themselves if they reach the cytoplasm as single elements. In our case, iron that potentially leaks out from the $MWCNTs_{+Fe}$, introduces a further degree of toxicity, even though this can also be due to the presence of nanotube aggregates, that is the dominant form of internalized unpurified samples.

A number of reports suggest an interaction between CNTs and the cytoskeleton. Walker et al. (2009) demonstrated marked actin filament and VE-cadherin disruption, cytotoxicity and reduced tubule formation after 24 hours exposure of human aortic endothelial cells to both MWCNTs and SWCNTs. Purified and dispersed SWCNTs have a great impact on cytoskeleton, reorganizing actin structures and inducing the formation of plaques of actin at the apical surface of HeLa cells (Holt et al., 2010). Moreover, in human fibroblasts treated with MWCNTs, the amount of stressed fibers decreased and became highly disordered, while, in control conditions, these structures are distributed at the wound edge of the cell. They are well ordered and orientated parallel to the direction of cell migration (Zhang et al., 2011). Since cytoskeletal proteins act as rails for vescicle transport, the granule mobility is constrained by the filamentous actin network. Changes in the actin viscosity will propel granules through the actin cortex (Garcia et al., 2006; Oheim et al., 2000). Thus, our hypothesis is that MWCNTs

entering the MCCs cause a partial disruption of the cytoskeletal structure, with a consequent slowdown of vesicles movement toward the plasmamembrane. Furthermore, our amperometric recordings clearly show a reduced frequency of released chromaffin granules without changes of their catecholamine granule content and kinetics of release. This suggests that MWCNTs internalization interferes with the secretory apparatus functionality with no effect on the mechanism of vesicles replenishment.

5. CONCLUSIONS

We provided evidence that MWCNTs enter MCCs after 24 h of exposure. Their internalization decreases the secretory response of chromaffin cells. In particular, MWCNTs reduce the overall exocytosis associated to an altered Ca^{2+}-dependence and the frequency of release, with no effects on vesicles content and kinetic of release of unitary events. MWCNTs purification with HCl (1 M), which preserves the size and morphology of the nanotubes, minimizes the amount of bioavailable iron impurities. This leads to reduced cellular uptake of the nanomaterial by chromaffin cells and milder depressive effects on secretion, uncovering the true significant toxic action of MWCNTs.

ACKNOWLEDGMENTS

We thank dr. Claudio Franchino for cell cultures preparation and technical support throughout all the experiments, dr. Sara Gosso, dr. Roberta Cesa and prof. Domenica Scarano for fruitful discussions.

Funding

This work was supported by the Regione Piemonte (CIPE 2005, grant # D14-2005 to E.C. and CIPE 2006, project NANOSAFE to B.F.) and by the San Paolo Foundation (Neuroscience Programme, grant # 2008.1155 to V.C.).

REFERENCES

Ali-Boucetta H, Al-Jamal KT, Müller KH, Li S, Porter AE, Eddaoudi A et al. Cellular uptake and cytotoxic impact of chemically functionalized and polymer-coated carbon nanotubes. Small 2011;7(22):3230-8.

Belyanskaya L, Weigel S, Hirsch C, Tobler U, Krug HF, Wick P. Effects of carbon nanotubes on primary neurons and glial cells. Neurotoxicology 2009;30(4):702-11.

Bertarione S, Bonino F, Cesano F, Jain S, Zanetti M, Scarano D et al. Micro-FTIR and Micro-Raman Studies of a Carbon Film Prepared from Furfuryl Alcohol Polymerization. Journal of Physical Chemistry B 2009;113, 10571-10574.

Bougrine ., Dupont-Pavlovsky ., Naji ., Ghanbaja J, Marˆeche´ JF, Billaud D. Influence of high temperature treatments on single-walled carbon nanotubes structure, morphology and surface properties. Carbon 2001;39, 685–695.

Carabelli V, Giancippoli A, Baldelli P, Carbone E, Artalejo AR. Distinct potentiation of L-Type Currents and Secretion by cAMP in rat chromaffin cells. Biophysical Journal 2003; 85, 1326–1337

Carabelli V, Marcantoni A, Comunanza V, De Luca A, Díaz J, Borges R et al. Chronic hypoxia up-regulates alpha1H T-type channels and low-threshold catecholamine secretion in rat chromaffin cells. J Physiol 2007;584(Pt 1):149-65.

Carabelli V, Gosso S, Marcantoni A, Xu Y, Colombo E, Gao Z et al. Nanocrystalline diamond microelectrode arrays fabricated on sapphire technology for high-time resolution of quantal catecholamine secretion from chromaffin cells. Biosens Bioelectron 2010;26(1):92-8.

Cesano F, Scarano D, Bertarione S, Bonino F, Damin A, Bordiga S et al. Synthesis of ZnO–carbon composites and imprinted carbon by the pyrolysis of ZnCl2-catalyzed furfuryl alcohol polymers. Journal of Photochemistry and Photobiology a-Chemistry 2008;196, 143-153.

Cheng C, Müller KH, Koziol KK, Skepper JN, Midgley PA, Welland ME, et al. Toxicity and imaging of multi-walled carbon nanotubes in human macrophage cells. Biomaterials 2009;30(25):4152-60.

Cho HG, Kim S, Lim HJ, Yun CH, Lee HS, Park CR. A simple and highly effective process for the purification of single-walled carbon nanotubes synthesized with arc-discharge. Carbon 2009;47 3544-3549.

Cravotto G, Garella D, Turci F, Gaudino E, Bertarione S, Agostini G et al. Rapid purification/oxidation of multi-walled carbon nanotubes under 300 kHz-ultrasound and microwave irradiation. New Journal of Chemistry 2011;35, 915-919.

Dresselhaus, M. S.; Jorio, A.; Souza, A. G.; Saito, R. Defect characterization in graphene and carbon nanotubes using Raman spectroscopy Philosophical Transactions Of The Royal Society A-Mathematical Physical And Engineering Sciences 2010;368 5355-5377.

Elgrabli D, Bella-Gallart S, Guerre-Chariol O, Robidel F, Rogerieux F, Boczkowski J et al. Effect of BSA on carbon nanotube dispersion for in vivo and in vitro studies. Nanotoxicology 2007;1:266–278.

Fenoglio I, Greco G, Tomatis M, Muller J, Raymundo-Piñero E, Béguin F et al. Structural defects play a major role in the acute lung toxicity of multiwall carbon nanotubes: physicochemical aspects. Chem Res Toxicol 2008;21(9):1690-7.

García AG, García-De-Diego AM, Gandía L, Borges R, García-Sancho J. Calcium signaling and exocytosis in adrenal chromaffin cells. Physiol Rev 2006;86(4):1093-131.

Gavello D, Vandael DH, Cesa R, Premoselli F, Marcantoni A, Cesano F et al. Altered excitability of cultured chromaffin cells following exposure to multi-walled carbon nanotubes. Nanotoxicology 2012;6(1):47-60.

Holt BD, Short PA, Rape AD, Wang YL, Islam MF, Dahl KN. Carbon nanotubes reorganize actin structures in cells and ex vivo. ACS Nano 2010;4(8):4872-8.

Kagan VE, Tyurina YY, Tyurin VA, Konduru NV, Potapovich AI, Osipov AN et al. Direct and indirect effects of single walled carbon nanotubes on RAW 264.7 macrophages: role of iron. Toxicol Lett. 2006;165(1):88-100.

Liu X, Guo L, Morris D, Kane AB, Hurt RH. Targeted removal of bioavailable metal as a detoxification strategy for carbon nanotubes. Carbon N Y 2008;46(3):489-500.

Lund LG and Aust AE. Iron mobilization from asbestos by chelators and ascorbic acid. Arch Biochem Biophys 1990;278(1):61-4.

Malarkey EB, Reyes RC, Zhao B, Haddon RC, Parpura V. Water soluble single-walled carbon nanotubes inhibit stimulated endocytosis in neurons. Nano Lett. 2008;(10):3538-42.

Marcantoni A, Carabelli V, Vandael DH, Comunanza V, Carbone E. PDE type-4 inhibition increases L-type Ca^{2+} currents, action potential firing, and quantal size of exocytosis in mouse chromaffin cells. Pflugers Arch 2009;457(5):1093-110.

Marcantoni A, Vandael DH, Mahapatra S, Carabelli V, Sinnegger-Brauns MJ, Striessnig J et al. Loss of Cav1.3 channels reveals the critical role of L-type and BK channel coupling in pacemaking mouse adrenal chromaffin cells. J Neurosci 2010;30(2):491-504.

Martinez MT, Callejas MA, Benito AM, Cochet M, Seeger T, Anson A et al. Sensitivity of single wall carbon nanotubes to oxidative processing: structural modification, intercalation and functionalisation. Carbon 41 2003;2247–56.

Martra G, Tomatis M, Fenoglio I, Coluccia S, Fubini B. Ascorbic acid modifies the surface of asbestos: possible implications in the molecular mechanisms of toxicity. Chem Res Toxicol 2003;16(3):328-35.

Muller J, Huaux F, Fonseca A, Nagy JB, Moreau N, Delos M et al. Structural defects play a major role in the acute lung toxicity of multiwall carbon nanotubes: toxicological aspects. Chem Res Toxicol 2008;(9):1698-705.

Nimmagadda A, Thurston K, Nollert MU, McFetridge PS. Chemical modification of SWNT alters in vitro cell-SWNT interactions. J Biomed Mater Res A 2006;76(3):614-25.

Oheim M and Stühmer W. Tracking chromaffin granules on their way through the actin cortex. Eur Biophys J 2000;29(2):67-89.

Pacurari M, Qian Y, Fu W, Schwegler-Berry D, Ding M, Castranova V et al. Cell permeability, migration, and reactive oxygen species induced by multiwalled carbon nanotubes in human microvascular endothelial cells. J Toxicol Environ Health A 2011;75(2):112-28.

Pulskamp K, Diabaté S, Krug HF. Carbon nanotubes show no sign of acute toxicity but induce intracellular reactive oxygen species in dependence on contaminants. Toxicol Lett 2007;168(1):58-74.

Vandael DH, Marcantoni A, Mahapatra S, Caro A, Ruth P, Zuccotti A et al. Ca(v)1.3 and BK channels for timing and regulating cell firing. Mol Neurobiol 2010;42(3):185-98.

Vandael DH, Zuccotti A, Striessnig J, Carbone E. Ca(V)1.3-driven SK channel activation regulates pacemaking and spike frequency adaptation in mouse chromaffin cells. J Neurosci 2012;32(46):16345-59.

Xu H, Bai J, Meng J, Hao W, Xu H, Cao JM. Multiwalled carbon nanotubes suppress potassium channel activities in PC12 cells. Nanotechnology 2009;20(28):285102-285111.

Walker VG, Li Z, Hulderman T, Schwegler-Berry D, Kashon ML, Simeonova PP. Potential in vitro effects of carbon nanotubes on human aortic endothelial cells. Toxicol Appl Pharmacol 2009;236(3):319-28.

Wang R, Mikoryak C, Li S, Bushdiecker D, Musselman IH, Pantano P et al. Cytotoxicity screening of single-walled carbon nanotubes: detection and removal of cytotoxic contaminants from carboxylated carbon nanotubes. Mol Pharm 2011;8(4):1351-61.

Zhang Y, Wang B, Meng X, Sun G, Gao C. Influences of acid-treated multiwalled carbon nanotubes on fibroblasts: proliferation, adhesion, migration, and wound healing. Ann Biomed Eng 2011;39(1):414-26.

TABLES

Table 1. Physico-chemical properties of MWCNTs

samples	Mean diameter (nm)	Mean Lenght (μm)	SSA (m^2/g)	Elemental analysis (% oxides)[c]	Iron potentially bioavailable[d] (% Fe_2O_3)	Amount of defects [e] I_D/I_G	Aggregates mean size in DMEM (z-average, nm)
MWCNT $_{+Fe}$	67±2[a]	1.12±0.05 [a]	60.3	Fe 0.50 ± 0.01 Al 0.04 ± 0.03 Co < d.l. Ni < d.l.	0.420 ± 0.001	0.34 ± 0.08	391.8[f] 378.1[g]
MWCNT$_{-Fe}$	70 ± 2 [b]	1.23±0.05 [b]	52.6	Fe 0.050 ± 0.001 Al 0.06 ± 0.03 Co < d.l. Ni < d.l.	0.002± 0.001	0.33 ± 0.09	467.3[f] 356.4[g]

a Gavello et al. 2012; b evaluated by TEM; c evaluated by means of AE-ICP spectrometry; d evaluated by measuring spectrophotometrically the amount of iron ions extracted by ferrozine/ascorbic acid system; e evaluated by means of Raman spectroscopy; f concentration: (263 mg/l); e concentration: (50 mg/l);

Table 2.

	Freq (Hz)	**$Q^{1/3}$ ($pC^{1/3}$)**	**Imax (pA)**	**$t_{1/2}$ (ms)**	**m (nA/s)**	**t_p (ms)**
Control (n=25)	0.47±0.07	0.56±0.02	35±5	8.5±0.9	15.2±2.5	5.1±0.4
$MWCNT_{-Fe}$ (n=13)	0.11±0.04	0.54±0.06	17.9±4.4	12.1±2.1	6.4±1.7	7.9±1.4
$MWCNT_{+Fe}$ (n=10)	0.07±0.01	0.53±0.06	16.6±3.8	9.6±2.2	6.9±2.0	5.5±1.4

Mean values (± s.e.) of amperometric spikes parameters, respectively indicating: frequency of release (Hz), cubic root of the quantal charge (pC^1/3), maximal spike amplitude (pA), half time width (ms), rise time (nA/s), time to peak (ms). Number of cells indicated in parenthesis in the first column.

FIGURE CAPTIONS

Figure 1. AFM topography images and height profiles of MWCNTs

5x5 μm nc-AFM topography images of: a) ground $MWCNTs_{+Fe}$ and b) ground $MWCNTs_{-Fe}$ solution at RT. The profiles shown in panels c) and d) are referred to two different $MWCNTs_{+Fe}$ of panel a) and to one $MWCNTs_{-Fe}$ of panel b), respectively. From these, it is possible to image isolated and bundled MWCNTs and a precise evaluation of their morphological properties (i.e. size, shape). In both cases shown in a) and b), the fragmented MWCNTs were AFM imaged after dilution in isopropyl alcohol, sonication for 10 minutes of the solution and subsequent dispersion on the mica support.

Figure 2. **Effect of purification on nanotubes defectivity**

Raman spectra of MWCNTs in the 500-4000 cm^{-1} range. In the inset an expansion of the 1550-1700 cm^{-1} region is shown. The dotted black line refers to ground MWCNTs ($MWCNT_{+Fe}$), and the continuous gray line to ground MWCNTs after iron removal ($MWCNT_{-Fe}$). The positions of the bands are indicated in the upper part of the figure. The lines are overlapped suggesting that the purification treatment does not affect the structure of the MWCNTs.

Figure 3. **Dispersion of $MWCNT_{-Fe}$ in cell media**

Analysis of the aggregation/agglomeration behavior of $MWCNT_{-Fe}$ (263 mg/l) in DMEM +15% FBS. a) Dinamic Light Scattering (DLS); the z-average curves correspond to three different measures on the same suspension during 15 minutes. The curves have a similar shape suggesting the suspension being stable during the time of the measurement. b) Optical microscopy; the image is a representative micrograph of the suspension. MWCNTs appears poly-dispersed with aggregates/agglomerates ranging from 0.3 to 10 micrometers in size.

Figure 4. Electron microscopy photographs of cultured RCCs with and without MWCNTs

a) Image of the cytoplasm of a control chromaffin cell in which are evident the secretory granules. b) A chromaffin cell exposed for 24 h to $MWCNTs_{-Fe}$. An aggregate is clearly visible in the cytoplasm, in the perinuclear region. c) High magnification of a RCC treated for 24 h with $MWCNTs_{-Fe}$. A single nanotube is crossing the nuclear membrane. d) Aggregates of $MWCNTs_{+Fe}$ and single nanotubes in the cytoplasm of a RCC. The internal organization of the cell is damaged. e) Comparison between the percentages of nanotubes internalization in cells

exposed to MWCNTs$_{+Fe}$ and MWCNTs$_{-Fe}$. After 24 h, nanotubes are present in 40% of RCCs exposed to MWCNTs$_{-Fe}$ versus 78% of RCCs exposed to MWCNTs$_{+Fe}$. f) Percentage of chromaffin cells having internalized MWCNTs$_{-Fe}$ inside them as single nanotubes (70%) or aggregates besides single nanotubes (30%). These percentages were normalized to the number of cells that internalized MWCNTs.

Figure 5. Depolarization-evoked secretion after MWCNTs exposure

a) Top: representative images of MCCs in control conditions (left), during exposure to MWCNTs$_{-Fe}$ (50 μg/ml, middle) and to MWCNTs$_{-Fe}$ (50 μg/ml, right). The black arrows indicate the example of selected cells for electrophysiological purposes. Below: capacitance increases (top) and Ca^{2+} current recordings (bottom) during step depolarizations to +10 mV from three representative MCCs: control condition (left), after 24 hour exposure to MWCNTs$_{-Fe}$ (50 μg/ml, middle) and after 24 hour exposure to MWCNTs$_{+Fe}$ (50 μg/ml, right). b) Mean capacitance changes measured in control conditions (black bar) and after exposure to different concentration of the two MWCNTs samples (-Fe, white bars, and +Fe, gray bars) at two different concentration, 50 and 263 μg/ml. Controls are significantly different from all the groups of treated cells ($p< 0.05$, one way ANOVA followed by Bonferroni post-hoc test). Moreover, there is a significant difference between MWCNTs$_{-Fe}$ (50 μg/ml) treated cells and MWCNTs$_{-Fe}$ treated cells (50 μg/ml) ($p< 0.05$, one way ANOVA followed by Bonferroni post-hoc test). c) Mean quantity of charge measured in control conditions (black bar) and after exposure to different concentrations of the two samples of MWCNTs (-Fe, white bars, and +Fe, gray bars) at two different concentration, 50 and 263 μg/ml. There are no significant differences between the groups.

Figure 6. ΔC distribution and altered Ca^{2+} -dependence during MWCNTs exposure

a) ΔC (fF) distributions for controls (left), MCCs exposed to MWCNT$_{-Fe}$ (middle) and MWCNT$_{+Fe}$ (right). Controls and MWCNT$_{-Fe}$ treated cells distributions were fitted with a double Gaussian function. b) Overlap of the three Gaussian fits: control (solid line), MWCNT$_{-Fe}$ (dashed line) and MWCNT$_{+Fe}$ (dotted line) c) Ca^{2+} dependence of exocytosis was determined by plotting ΔC (fF) vs the corresponding Ca^{2+} charge density (pC). The slope of the linear regression under control conditions (filled squares, solid line) is statistically different from MWCNT$_{-Fe}$ (empty circles, dashed line) by 1 standard deviation and from MWCNT$_{+Fe}$ (triangles, dotted line) by 2 standard deviations.

Figure 7. Amperometric recordings of unitary secretory events

Amperometric spikes were evoked using 30 mM KCl-enriched external solution and recorded for 120 seconds, either under control conditions (a), or during exposure to $MWCNT_{-Fe}$ (b) and $MWCNT_{+Fe}$ (c), respectively. Insets show representative spikes (indicated by the asterisk) using an expanded time-scale.

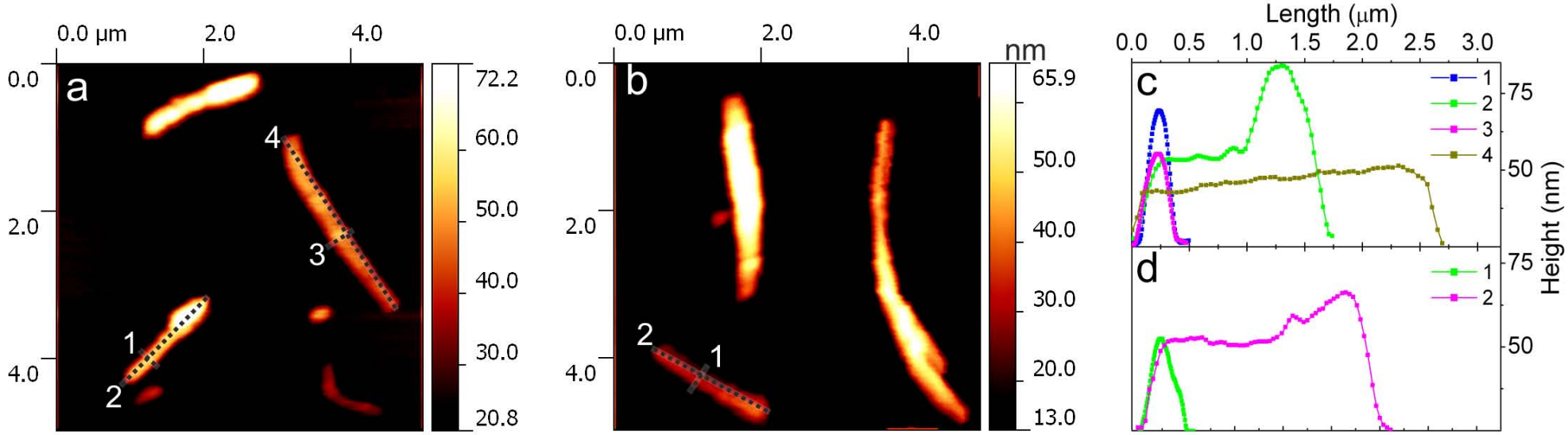
a
b
c
d
0.0 µm
2.0
4.0
0.0
2.0
4.0
nm
72.2
60.0
50.0
40.0
30.0
20.8
65.9
50.0
40.0
30.0
20.0
13.0
1
2
3
4
Length (µm)
0.0
0.5
1.0
1.5
2.0
2.5
3.0
75
50
Height (nm)

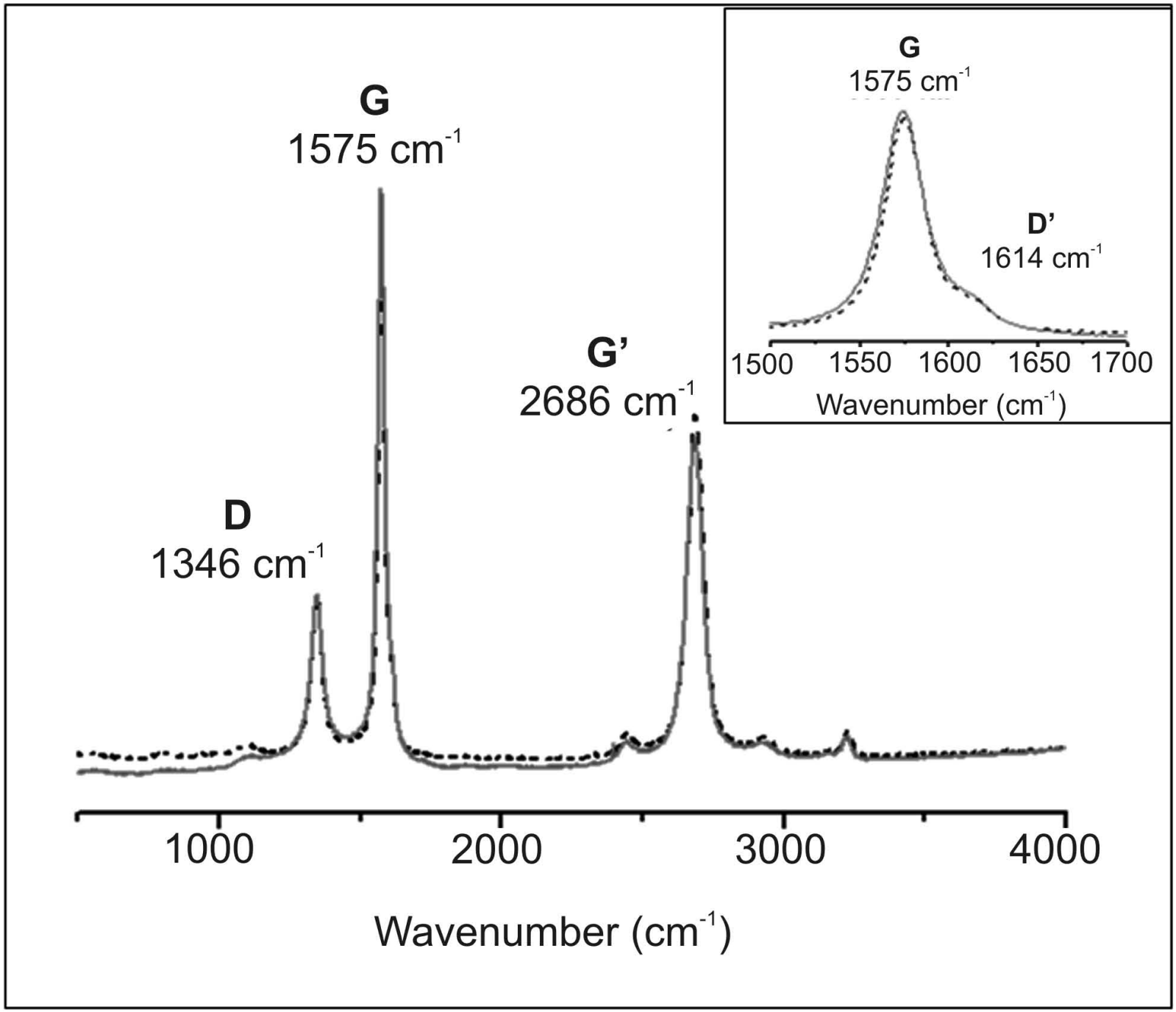
G
1575 cm-1
G'
2686 cm-1
D
1346 cm-1
1000
2000
3000
4000
Wavenumber (cm-1)
G
1575 cm-1
D'
1614 cm-1
1500
1550
1600
1650
1700
Wavenumber (cm-1)

Fig. 2

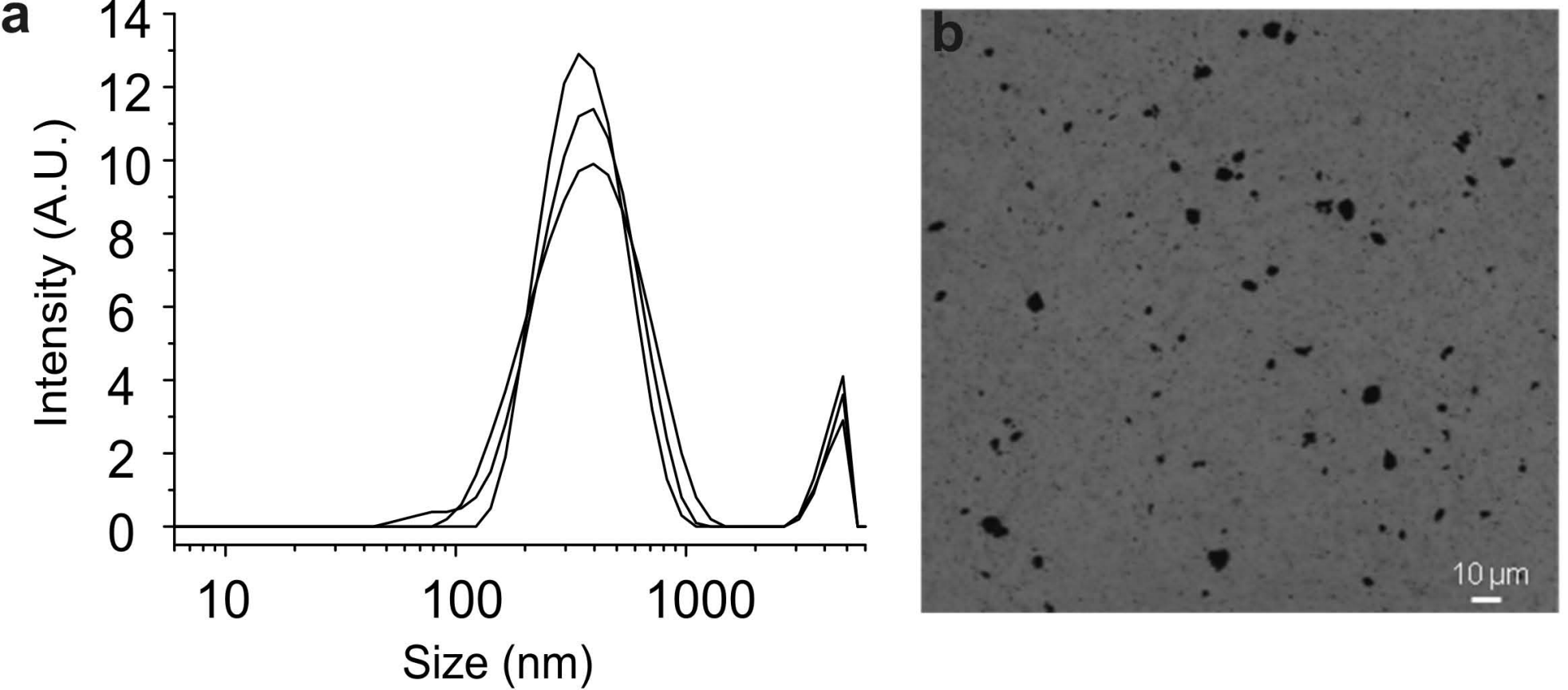

Fig. 3

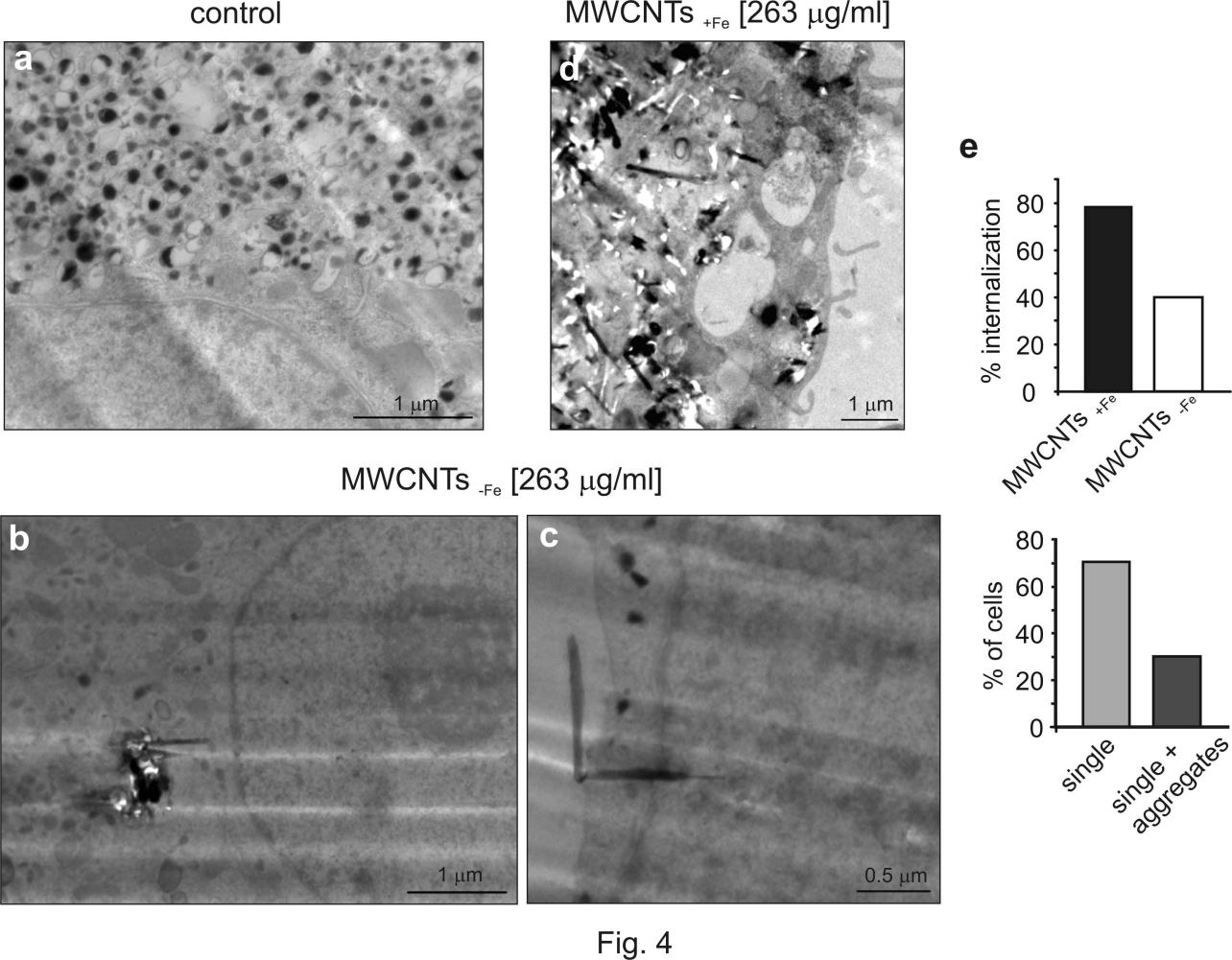
control
MWCNTs +Fe [263 μg/ml]
a
1 μm
d
1 μm
e
% internalization
80
60
40
20
0
MWCNTs +Fe
MWCNTs -Fe
MWCNTs -Fe [263 μg/ml]
b
1 μm
c
0.5 μm
% of cells
80
60
40
20
0
single
single + aggregates

Fig. 4

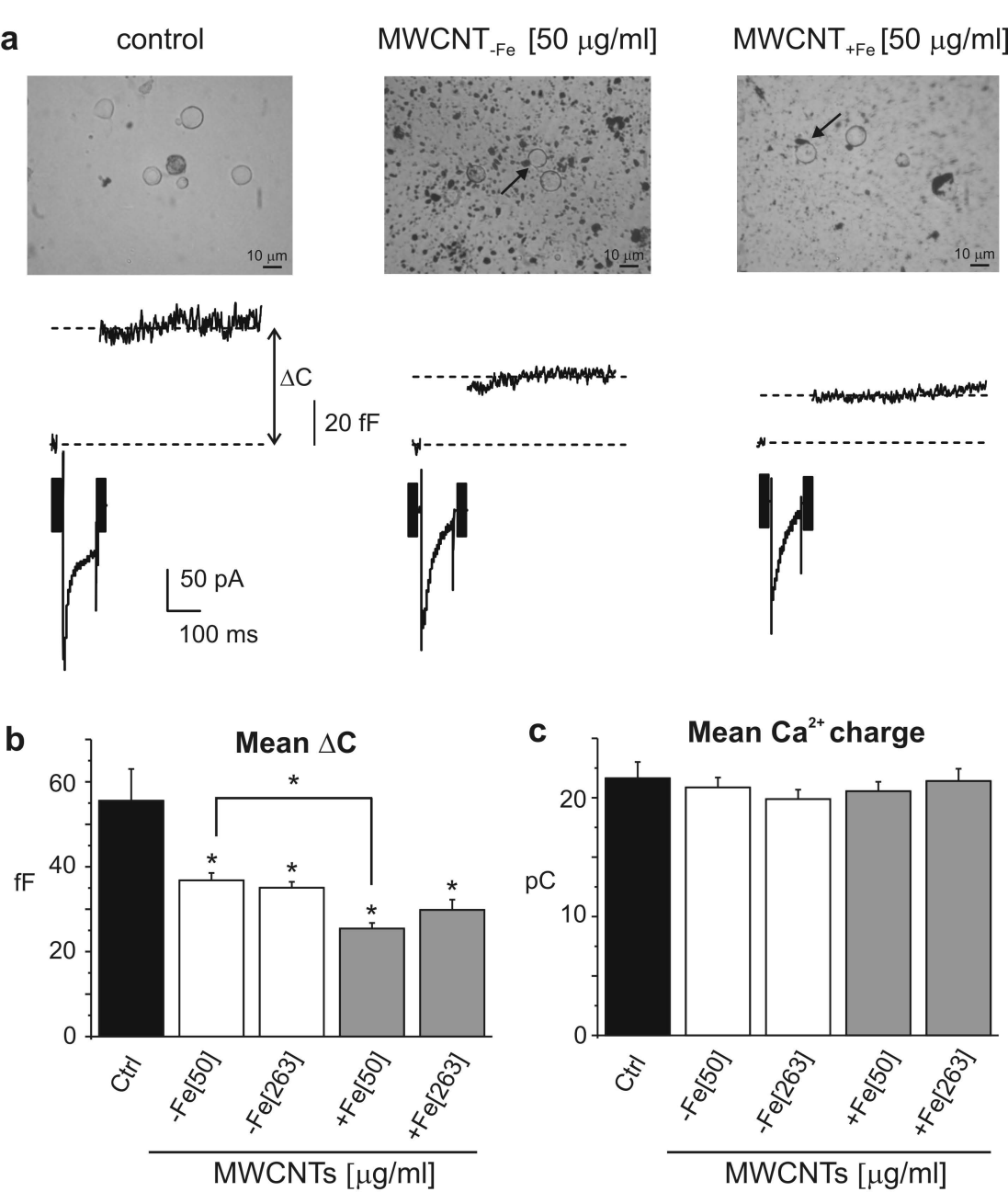
a
control
MWCNT-Fe [50 μg/ml]
MWCNT+Fe [50 μg/ml]
10 μm
10 μm
10 μm
ΔC
20 fF
50 pA
100 ms
b
Mean ΔC
fF
60
40
20
0
Ctrl
-Fe[50]
-Fe[263]
+Fe[50]
+Fe[263]
MWCNTs [μg/ml]
c
Mean Ca2+ charge
pC
20
10
0
Ctrl
-Fe[50]
-Fe[263]
+Fe[50]
+Fe[263]
MWCNTs [μg/ml]

Fig. 5

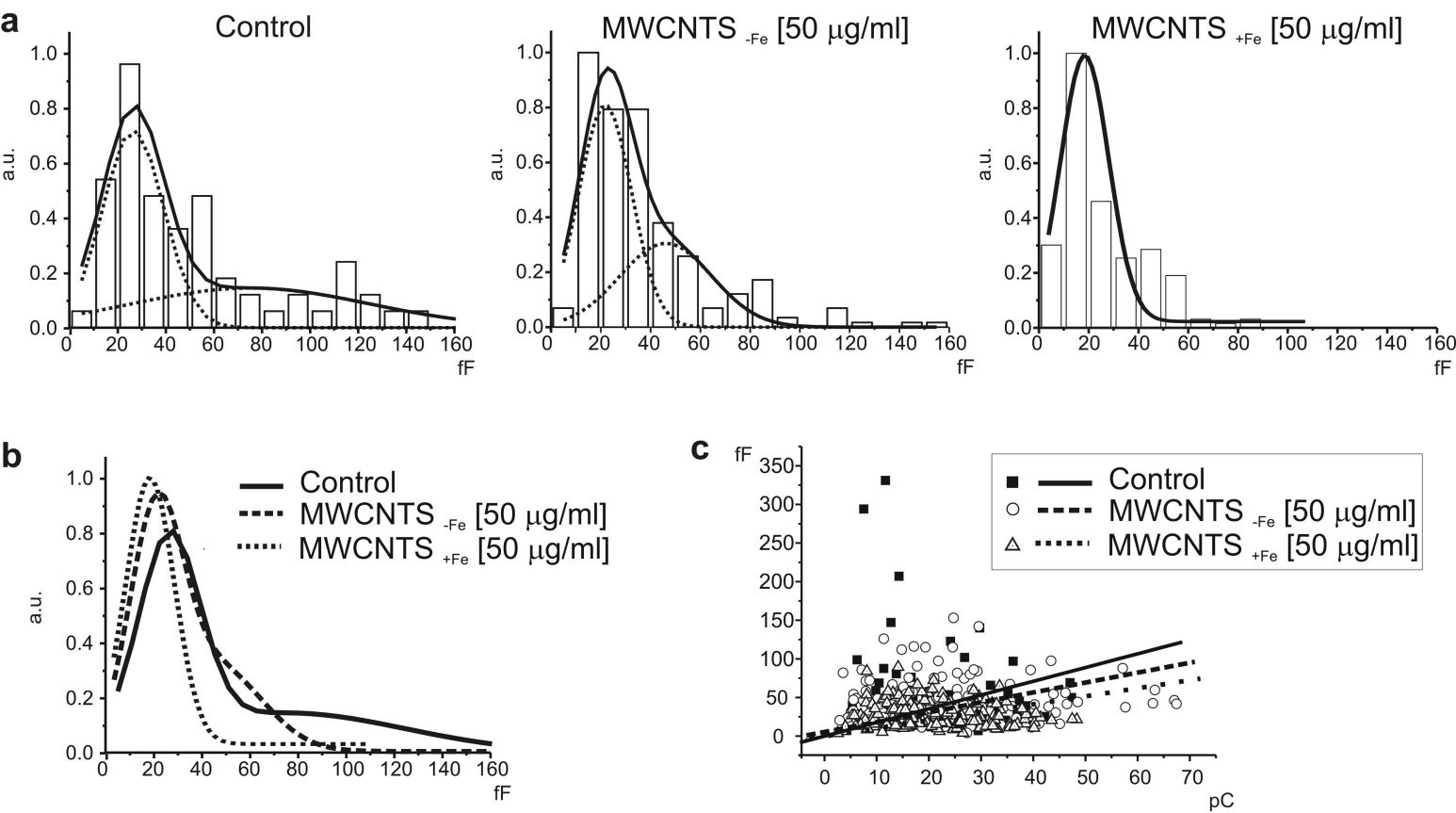
a
Control
MWCNTS -Fe [50 μg/ml]
MWCNTS +Fe [50 μg/ml]
a.u.
fF
b
Control
MWCNTS -Fe [50 μg/ml]
MWCNTS +Fe [50 μg/ml]
a.u.
fF
c
fF
pC
Control
MWCNTS -Fe [50 μg/ml]
MWCNTS +Fe [50 μg/ml]

Fig. 6

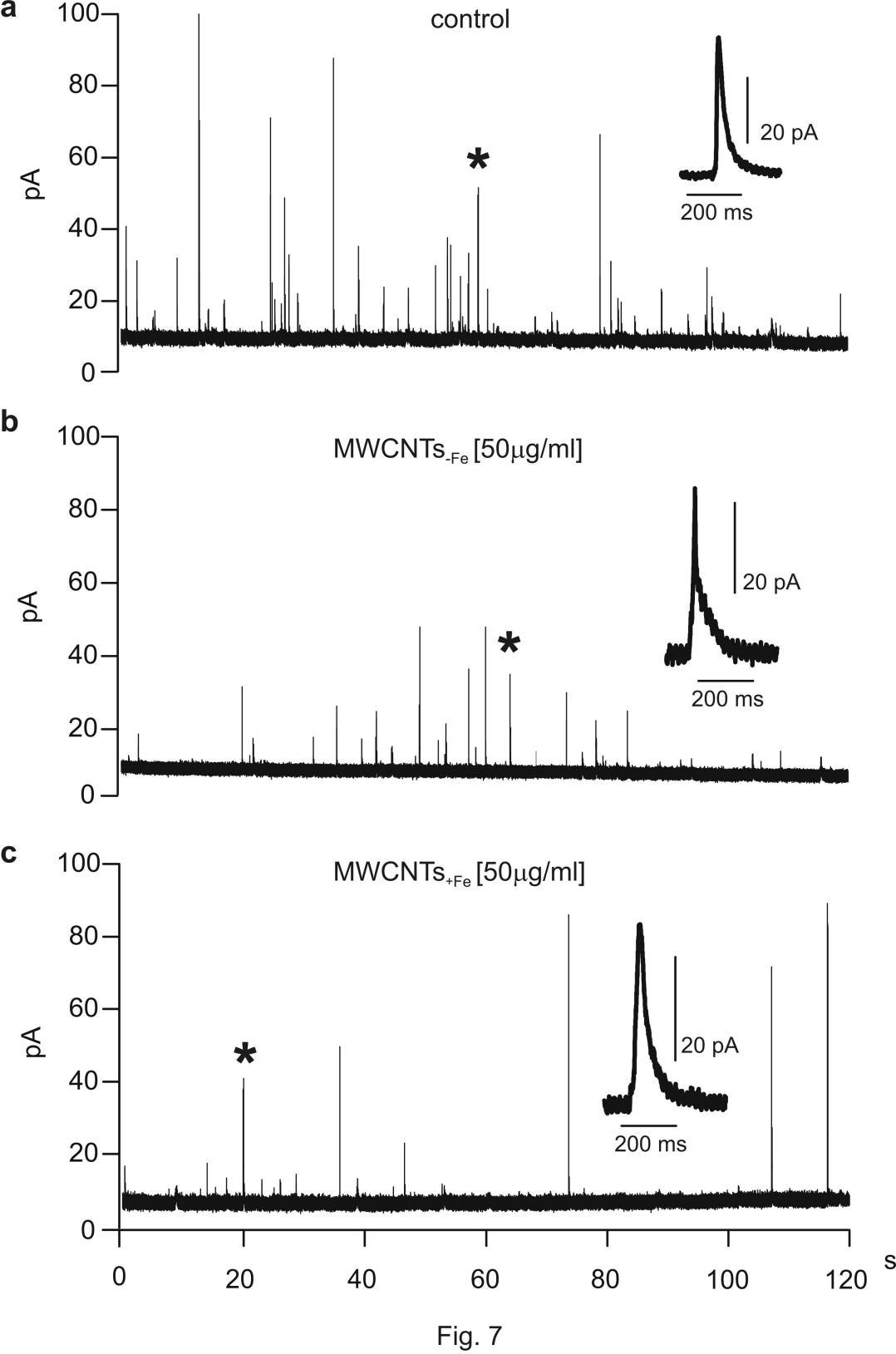
a
control
pA
100
80
60
40
20
0
20 pA
200 ms
b
MWCNTs-Fe [50μg/ml]
pA
100
80
60
40
20
0
20 pA
200 ms
c
MWCNTs+Fe [50μg/ml]
pA
100
80
60
40
20
0
20 pA
200 ms
0
20
40
60
80
100
120
s

Fig. 7